Todorovic, J., Torsæter, M., Opedal, N., Wiese, B., Martens, S. (2014): Characterization of CO2 Pipeline Material from the Ketzin Pilot Site. - *Energy Procedia*, *63*, p. 2610-2621.

DOI: http://doi.org/10.1016/j.egypro.2014.11.283

Available online at www.sciencedirect.com

ScienceDirect

Energy Procedia 63 (2014) 2610 – 2621

Energy Procedia

GHGT-12

Characterization of CO_2 Pipeline Material from the Ketzin Pilot Site

Jelena Todorovic[a]*, Malin Torsæter[a], Nils Opedal[a], Bernd Wiese[b] and Sonja Martens[b]

[a] *SINTEF Petroleum Research, 7031 Trondheim, Norway*
[b] *GFZ German Research Centre for Geosciences, Telegrafenberg, 14473 Potsdam, Germany*

Abstract

Due to lack of relevant field data it is difficult to predict with sufficient accuracy the corrosion rates and CO_2 flow in pipelines. Laboratory experiments are usually of short duration at small scales, failing to reproduce events such as repeated shutdowns. It is therefore important to learn from CO_2 storage pilot sites, and the present paper reports characterization of stainless steel pipeline material from Ketzin. It was exposed to CO_2 flow for about five years, including several shut-ins, and samples were collected from straight and bent sections with different proximity to heaters of the injection facility. The samples displayed no visual signs of severe corrosion, but were investigated in detail using scanning electron microscopy and a profilometer. This revealed that prolonged CO_2 flow had roughened the inner pipe surfaces and caused some intergranular and pitting corrosion, especially close to heaters and in bent pipe sections.

Peer-review under responsibility of the Organizing Committee of GHGT-12

Keywords: CO_2 transport; pipelines; corrosion; pipe surface topography

1. Introduction

CO_2 Capture and Storage (CCS) is today considered one of the most important technologies for reducing global emissions of greenhouse gases. The International Energy Agency's two-degree scenario involves using CCS to reduce the world's CO_2 emissions by about seven gigatonnes per year in 2050 [1]. This amount is significantly larger than the 50 megatonnes currently used for enhanced oil/gas recovery purposes [2]. Larger transported volumes imply

* Corresponding author. Tel.: +47 93003592.
E-mail address: jelena.todorovic@sintef.no

Peer-review under responsibility of the Organizing Committee of GHGT-12
doi:10.1016/j.egypro.2014.11.283

that there is a potential high benefit of more precise knowledge of the corrosive behavior and flow of CO_2. This can aid the choice of pipe materials and operational parameters, and can thereby improve CCS safety and cost efficiency.

The *lack of relevant field data* has been pointed out as the key obstacle for accurately modelling the corrosive behavior and flow of CO_2 in pipelines [3,4]. Laboratory experiments are usually done at small scales and with short durations, compared to what is the case in field situations [5,6]. It is also difficult to reproduce large-scale pipeline events in the lab, such as start-up and shut-ins. In most field situations, the CO_2 pipeline flow is also expected to fluctuate since coal- and gas-fired power plants are operated in response to external demands. By replacing this transient flow pattern with a steady-state one in the laboratory, all effects of pressure, temperature and phase changes inside the pipeline will be neglected [7]. For the pipeline material, the effects of depressurization (either planned or accidental) will be rapid cooling and possibly dry ice formation [8]. This can damage pipes and/or coatings e.g. by making them brittle and vulnerable to cracking [4].

Field data is also necessary to understand the effects of various types and amounts of impurities on CO_2 flow and corrosive behavior. Depending on the CO_2 source and capture process, the pipeline flow might contain nitrogen, oxygen, water, sulfur oxides, methane and other substances [4]. Even if they are only present in small amounts, these impurities can significantly alter the thermodynamic and transport properties of the CO_2 mixture [9].

An optimal way to obtain relevant field data is to look at CCS pilot sites. The scope of this paper is to present a detailed characterization of the CO_2 transport pipeline gathered from the Ketzin pilot site during decommissioning of the injection facility. As will be explained in the following, the pipes have been exposed to prolonged CO_2 flow over a period of about five years. We employ several scanning electron microscopy (SEM) techniques and a profilometer to map the effects of CO_2 flow on pipe surface chemistry/composition and topography. The collected data is valuable input for modelling of CO_2 pipeline flow and corrosive behavior and it can shed light on many of the knowledge gaps discussed above.

2. Pipeline sampling at Ketzin

The Ketzin pilot site in Germany, which is now to be abandoned, is the longest operating onshore CO_2 storage site in Europe [10, 11]. Injection of CO_2 began in June 2008 and ended in August 2013. During this period, a total amount of 67 kilotonnes of CO_2 was safely injected into a saline aquifer at a depth of 630 m - 650 m. The injection facility was a special set-up for the pilot site and comprised of two intermediate storage tanks, plunger pumps and an electrical heater to heat up the liquid CO_2 from -18 °C, as delivered by trucks and stored in the intermediate storage tanks, to the desired injection temperature of about 35 °C [12]. Four ambient air heaters were located upstream of the electrical heater to pre-heat the CO_2 and to reduce the electrical power need. The pipeline which was sampled for this study connected the injection facility and its heaters with the injection well Ktzi 201. Total length of pipeline was about 100 m. The pipeline was disassembled during decommissioning in December 2013. The locations where the samples were collected and the temperature and CO_2 phase conditions during standard operation are summarized in Table 1. The bending angle of all bent pipe sections was 90°.

Table 1. A summary of the different pipeline samples collected at the Ketzin pilot site.

Sample	Location	Temperature during standard operation	CO_2 phase conditions	Pipe type	Date sampled
1	Inlet of ambient air heater	~ -15 °C	liquid	bent	09.12.2013
2	Outlet of ambient air heater	Ambient air temperature, mostly 5 to 20°C	liquid	bent	09.12.2013
3	~ 45 m behind electrical heater	~ 35 to 45°C	gaseous	straight	10.12.2013
4	~ 95 m behind electrical heater	~ 30 to 40°C	gaseous	straight	11.12.2013

The studied pipe samples had been exposed to CO_2 flow for approximately five years. The ambient air heaters (samples 1 and 2) were added in November 2008 after the injection had already started in June 2008. Hence, the samples 1 and 2 have been exposed to the CO_2 about five months less than samples 3 and 4.

Besides standard operation with conditions as shown in Table 1, CO_2 of higher temperature (up to ~80°C) has passed in single cases the pipeline where samples 3 and 4 were taken. According to the monitoring data, this occurred about once a month for several minutes. In addition, there was a period of ten days in 2008 when CO_2 temperatures were about 60°C.

Moreover, a cold-injection experiment was conducted between March and July 2013. Here, the injection temperature was stepwise reduced from 45°C down to 10°C to study the thermodynamics in the wellbore and its impact on the reservoir [13]. A total amount of 3 kt of CO_2 was injected throughout this experiment. Down to a temperature of 25 °C the entire injection process continued to occur single-phase with gaseous CO_2. At an injection temperature of 20 °C, the CO_2 started to condense liquid CO_2 droplets and the injection process occurred under two-phase conditions in the surface installations where samples 3 and 4 were taken. The ambient air heaters where samples 1 and 2 were gained were not in operation during the experiment.

The total injection period included several shut-in phases of different durations for downhole monitoring campaigns, research demands or nearby drilling activities. During shut-ins, the pipeline was at ambient temperature and valves between the injection well Ktzi 201 and the pipeline were closed.

The CO_2 flowing through the pipeline originated from two different sources:

- 65.5 kt of CO_2 (purity > 99.9%) from Linde AG.
- 1.5 kt of CO_2 (purity > 99.7%) from the oxyfuel pilot "Schwarze Pumpe" (Vattenfall) in May-June 2011.

Two types of stainless steel of austenitic 300 series were used in the pipeline. Austenitic stainless steels contain a minimum of 16% chromium, a maximum of 0.15% carbon and sufficient nickel and/or manganese to retain an austenitic structure at all temperatures from the cryogenic region to the melting point of the alloy. Traces of other elements, like silisium, nitrogen, phosphorus and sulphur are also common. A passive film of chromium oxide is what prevents the surface from corroding as fast as ordinary steel. The sampled pipeline material was of grade 1.4301/304, with a diameter of 33.70 mm and wall thickness of 2.60 mm.

3. Experimental details

3.1. Sample preparation

Pieces of approximately 1 cm × 1 cm were cut from the pipes using a motorized saw blade. Care was taken to avoid any contamination; however, it was necessary to use water during the cutting to avoid damage from heat generation. From the two straight pipe sections, samples were cut from pipe top and bottom. This was done to investigate any possible effects of gravitational separation of the flow. The two bent pipes samples were taken from the sharp and blunt sides of the pipe bend. These two surface locations were chosen to be able to observe any potential effects the fluid velocity could have on pipe surface alteration. The parts of the CO_2 pipeline sections that were compared in this work are schematically summarized in Fig. 1.

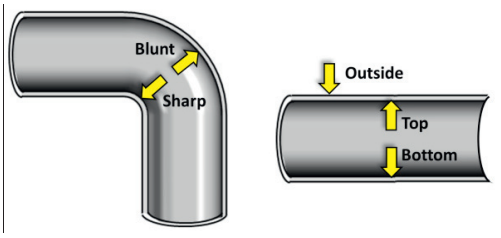

Fig. 1. A schematical illustration of the different pipe surface locations that were compared in the analysis.

3.2. Surface characterization methods

To avoid heat damaged zone at the sample edges induced by cutting, each sample was investigated in the central region – a few mm away from the edges. A Veeco Dektak 150 profilometer was used to measure surface profiles and to determine the roughness of surfaces. This instrument is a contact stylus profilometer. A 12.5 μm diamond tip stylus is run over a sample surface and records height differences which are plotted as a line profile. Height range of 65.5 μm or 524 μm was used, depending on surface curvature and roughness. A lateral resolution was 0.167 μm, that is 1 mm scanned in 20 s. Scan lengths were 5 mm or 1-3 mm for more curved surfaces. The Dektak software provides a wide range of analytical functions, of which average roughness and peak-to-valley distance functions were used. It is important to notice that the line scans are most reliable if run across a flat pipe surface. This was possible to approach for the straight sections of the pipes (samples 3 and 4) by scanning along the pipe as precisely as possible. However, the bent sections (samples 1 and 2) were more challenging, since the stylus measures also the surface curvature. The curvature severely affects the surface roughness values, which can be seen in a huge variation of roughness between the measurements for blunt section of samples 1 and 2. Therefore, left-over pieces (side-pieces remaining after cutting top/bottom and blunt/sharp sections) of samples 1 and 2 were scanned as well, since these had less curved regions. For control, left-over pieces of samples 3 and 4 were also scanned.

The pipe surfaces were also investigated using Scanning Electron Microscopy (SEM), Energy Dispersive X-ray Spectroscopy (EDX) and Auger spectroscopy. The instruments used were Hitachi TM3000 Tabletop SEM and JEOL Field Emission Auger Microscope JAMP-9500F. Hitachi SEM operates only in the backscattered electron (BSE) mode. Intensity in the BSE images depends on the average atomic number in the probed volume (the higher the atomic number the brighter the image). Hitachi SEM was operated at 5 kV for more surface sensitive imaging, and at 15 kV for imaging and EDX analysis. The Jeol Auger Microscope was operated at 10 kV and 15 kV in secondary electron (SE) mode. For acquisition of Auger spectra, the sample was tilted for 30°. The Auger process involves relaxation of electrons to a lower unoccupied level (created by ionization by an incident electron) accompanied by emission of another electron from a higher level. For example for a $KL_1L_{2,3}$ transition, the kinetic energy of the electron emitted from $L_{2,3}$ is calculated as:

$$E_{kin} = E_K - E_{L1} - E_{L2,3} \tag{1}$$

where E_K, E_{L1} and $E_{L2,3}$ are binding energies of electrons with respect to the vacuum level. The emitted electrons are detected and their number is plotted with respect to the kinetic energy. Auger spectroscopy is an extremely surface sensitive technique, probing only a few nm deep into a material.

4. Results

4.1. Visual inspection of pipe surfaces

By visual inspection of pipe edges after cutting, it was observed that neither erosion nor corrosion penetrates deep into the bulk stainless steel. Figure 2 shows optical microscope images of inner surfaces of all four samples and outer surface of sample 2. It is apparent that the pipes have different appearance of inner and outer surfaces. The outer surface (Fig. 2c) has more scratches and is metallic grey in colour. All inner surfaces have a slightly different colour. Otherwise, no visual signs of corrosion were observed. The bent section of sample 1 (Fig. 2a,b) exhibited a different colour on the inside (brownish to dark grey) compared to the other samples (grey). This can be due to welding or pipe bending prior to CO_2 flow. In addition, the inner surface of sample 1 at the bent section appeared to have distinct dark lines along the flow direction. On the inner surface of sample 2 (Fig. 2d) some similar weak lines can also be observed. This is in contrast to samples 3 and 4 (Fig. 2e,f), which both seem to have a homogeneous roughness.

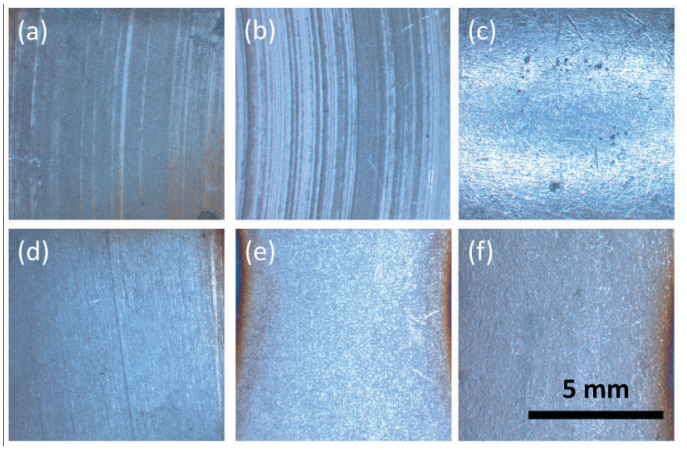

Fig. 2. Optical images of the pipes after cutting: (a) Sample 1 sharp section, inner surface, (b) sample 1 top section, inner surface, (c) sample 2 blunt section, outer surface, (d) sample 2 sharp section, inner surface, (e) sample 3 top section, inner surface, (f) sample 4 top section, inner surface.

The samples were further inspected with a slide caliper to investigate the wall thickness of the samples. Table 2 shows the thickness of the pipe walls measured at the location where the 1x1 cm SEM samples were taken from. The measurements did not reveal any major differences between the top and bottom wall thickness for any of the pipes or samples types. As seen, a difference in the wall thickness was observed between the sharp and blunt walls for the bent pipes. This probably is caused by the bending, since the difference in thickness is larger than the determined corrosion depth.

Table 2. Measured pipe thickness at the location where SEM/profilometer samples were taken. Values given in millimeters.

Pipe type	Sample number	Location of samples			
		Top	Bottom	Sharp	Blunt
Bent	1	2,58 ± 0,02	2,66 ± 0,04	2,81 ± 0,06	2,43 ± 0,04
	2	2,89 ± 0,01	2,76 ± 0,03	3,05 ± 0,01	2,44 ± 0,02
		Top	Bottom	Side	Side
Straight	3	2,71 ± 0,04	2,55 ± 0,05	2,49 ± 0,04	2,70 ± 0,04
	4	2,61 ± 0,01	2,62 ± 0,02	2,57 ± 0,02	2,61 ± 0,01

4.2. SEM study of pipe surfaces

Despite little corrosion being visible by optical inspection, at higher magnification, SEM revealed that the pipe surfaces had in fact been affected by the prolonged CO_2 flow. No new pipeline material, unexposed to outer conditions or CO_2, was available for comparison. So for a reference, outer surfaces of samples 2 and 4 were studied by SEM. During injection, this surface had been exposed to the outer conditions instead of CO_2. As seen from Fig. 3 on the left, the outer surface of the sample 2 (similar for sample 4) has a high density of seemingly deep, large pits (up to few hundreds of µm long) in between rather smooth regions. But there are traces of intergranular corrosion in these smooth regions as well. This is indicated by the tiny cracks in between the steel grains where loss of material occurred and/or corrosion products precipitated (darker regions), Fig. 3 on the right. Otherwise, we assume that this is how the inner pipe surface used to appear before the CO_2 injection started.

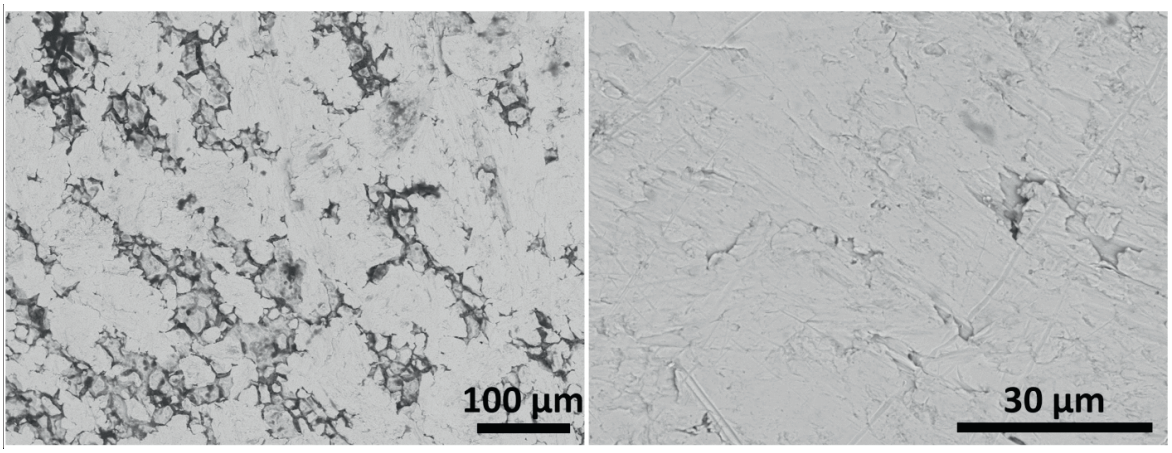

Fig. 3. BSE images at two different magnifications of the outer surface, that has not been in contact with CO_2, of the blunt sample 2.

Several regions of the inner surface of the CO_2 transport pipeline were also analyzed by SEM, and the results are summarized in Fig. 4. For samples 1 and 2, the sharp and blunt bent sections are compared, while for samples 3 and 4 the top and bottom sections of straight pipe sections are compared. The location in the pipe is indicated in the top right corner of each figure. As seen from this overview figure, all samples display a cracked surface layer, which is typically the first sign of onset of corrosion. Intergranular corrosion, with loss of material in between grains, is also visible in all the samples. Overall, sample 1 has the most corroded inner surface – followed by sample 2. The grooves in the cracked surface layer appear to be shallowest in sample 4.

There are little differences in corrosive attack between the sharp and blunt sections of the bend in samples 1 and 2. For sample 1, the sharp section had a higher density of dark/brownish lines than the blunt one (also visible by eyes/in optical microscope, Fig.2), but the degree of corrosion was similar. In Fig. 4, a transition between a dark line and lighter region in between the lines is shown from sample 1. Corrosion degree of both sharp and blunt sections of sample 2 appears similar to samples 3 and 4, except that the grooves seem to be deeper. Further, as Fig. 4 displays, there was little or no difference in corrosion between the top and bottom sections of the straight pipes (samples 3 and 4) which were overall less attacked by corrosion than the blunt and sharp sections of samples 1 and 2.

Higher magnification BSE images in Figure 5 show different types and degrees of corrosion observed in the four samples. This figure depicts especially corroded areas. Sample 1 is dominated by strong intergranular corrosion, while for sample 2, deep grooves of intergranular corrosion are visible. Sample 3 displays signs of intergranular corrosion as well, but the grooves are not especially deep. For sample 4, some shallow intergranular corrosion was observed. Not all grains were separated in samples 3 and 4 – so what we observe is most likely only the onset of intergranular corrosion. The micro-sized holes or craters on grain surfaces (not at their boundaries) confirm that there is also some pitting corrosion on most of the surfaces. Some large pitting craters are visible for sample 1 (Fig. 5a), and some smaller and more shallow ones for samples 2, 3 and 4 (Figs. 5b,c,d). The particles (dark) in between or on top of the grains, as seen in Fig.5(a,c) may be corrosion products or contamination or both.

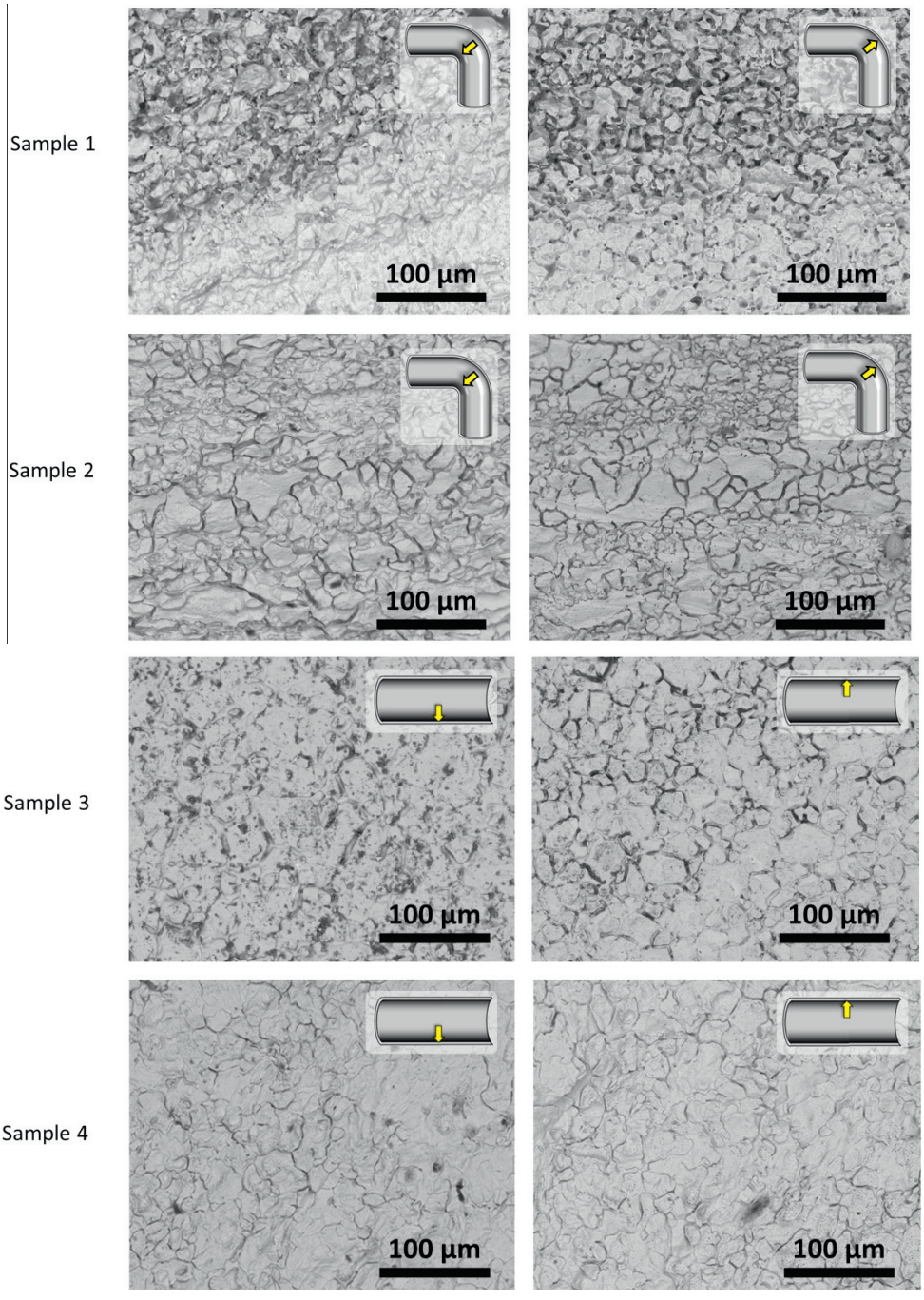

Fig. 4. BSE images of the inner surfaces of all the samples described in Table 1. For the bent pipe samples the sharp and blunt section of the bend is compared, while for the straight pipe samples the top and bottom section of the pipe is compared.

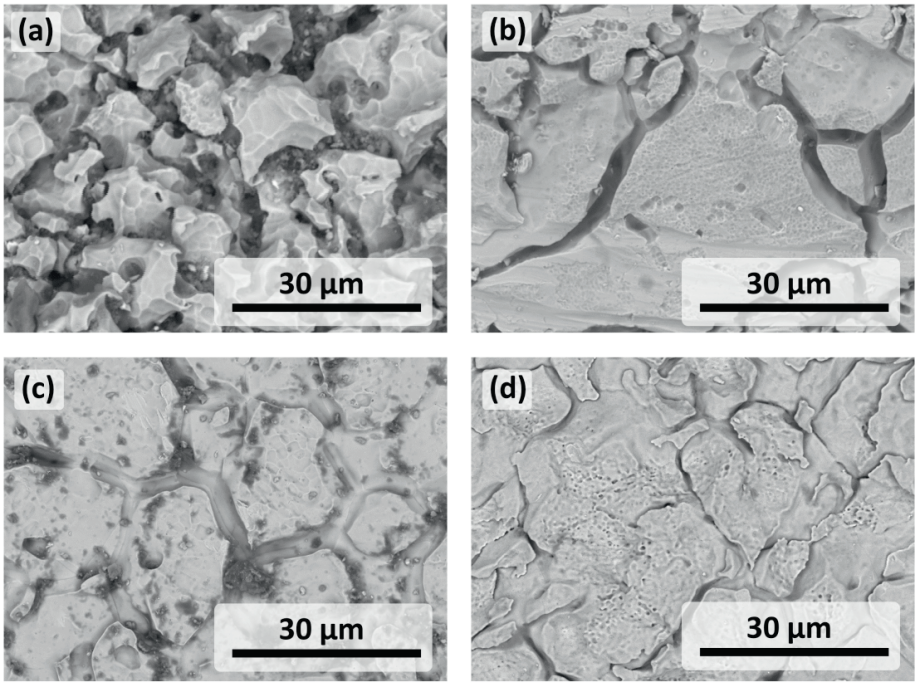

Fig. 5. High magnification SEM images of the most corroded regions of the inner surface for each of the samples. (a) Sample 1, (b) Sample 2, (c) Sample 3 and (d) Sample 4.

4.3. Compositional measurements

The surface composition of the different samples was studied by two analytical techniques, EDX and Auger spectroscopy. Both techniques confirmed the elements present in the stainless steel grade used in the pipeline, and revealed that all samples contained some carbon on the surface. Figure 6 depicts typical EDX maps from the pipeline with the most abundant elements in addition to carbon and oxygen. The latter two were included as they were the main constituents of the corrosion products or possible contamination or protective oxide layer on the surface. The main elements (Fe, Ni, Cr) are present overall, i.e. their EDX maps are matching well the corresponding BSE image in Fig.6. However, overall weak O signal (with specific spots of higher counts) indicates depletion of the protective chromium oxide layer, which is characteristic for ongoing surface corrosion. The carbon could originate from contamination or corrosion products or both. Note that it is impossible to determine the exact composition of possible corrosion products by using only EDX in SEM.

The surface composition of sample 3 was analyzed using Auger spectroscopy, and the results are depicted in Fig. 7. Initially, strong C peak and weaker O peaks were dominating the Auger spectrum (Fe, Cr and Ni not detected), indicating carbon contamination at the surface. After 8 minutes of sputtering to clean the sample, C peak was drastically reduced. Fe, Ni and Cr peaks then emerged, but Cr and O peaks were rather weak compared to Fe and Ni. The opposite would be expected if chromium oxide layer was preserved on the surface. The weak Cr and O peaks at the surface indicate that the protective chromium oxide layer has been damaged or even completely eroded. This is in line with the EDX results.

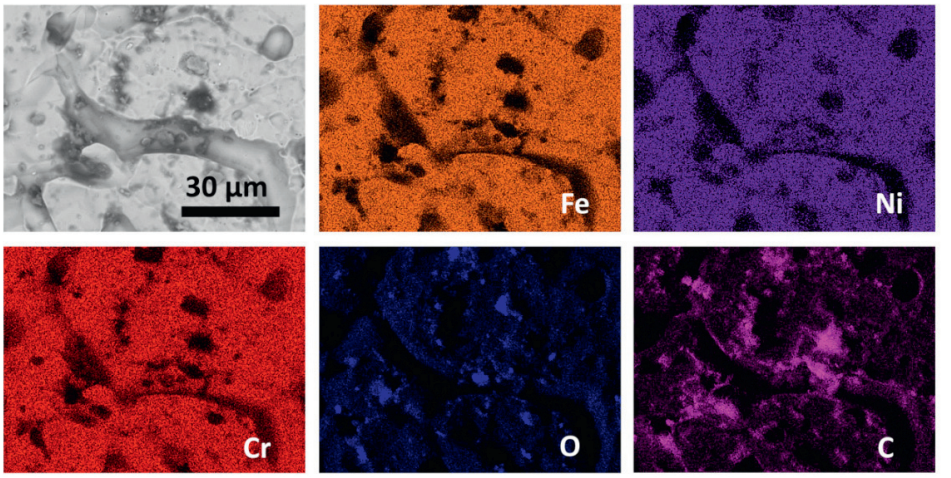

Fig. 6. BSE image and EDX mapping of the inner surface of sample 3. The main elements in the stainless steel are included in the mapping. Oxygen and carbon are shown as well, as these were prominent in the oxide layer and corrosion products/contamination.

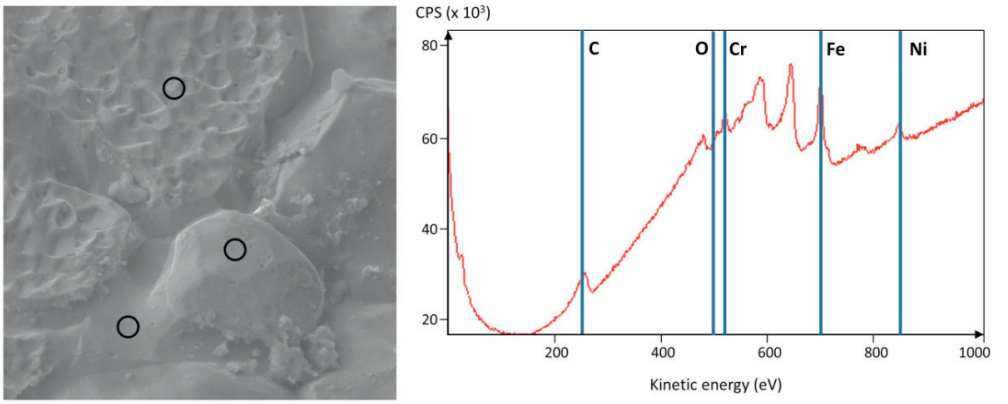

Fig. 7. SEM image of sample 3 indicating points on the surface analyzed by Auger spectroscopy. All points gave spectra similar to that depicted on the right, where the main peaks of the elements are marked with blue lines. Secondary (lower energy) peaks of Fe, Cr and Ni are not denoted.

4.4. Measurements of surface roughness

The outer surface roughness was measured on all four samples, and the obtained values for average roughness were quite consistent for all samples and falling within 1.5 – 2 µm. The inner surface roughness values are summarized in Table 3. The average roughness and peak-to-valley distance were calculated in Dektak software for a manually selected range of length (which may be the whole scanned length or less). Assuming a flat initial surface, the measured peak-to-valley distance reflects the depth of corrosion, with limitation in resolution by the stylus diameter. Namely, for sample 2, the grooves between the grains appear deep but they are narrow (≤ 5 µm, see Fig. 5), so peak-to-valley distance is smaller than for samples 3 and 4 which are less corroded.

A typical surface height profile, represented by sample 4, and surface profile across the dark/light lines for sample 1 are shown in Figure 8. Here sample 4 represents the case where roughness is independent of CO_2 flow direction (samples 2, 3, 4). The average peak-to-valley distance was about 20 µm, which is an estimate of corrosion depth.

Sample 1 had a similar height profile to sample 4 when scanned along dark lines or in between them, as seen in Fig. 2(a,b). However, when scanned across the lines, the profile changes drastically, as seen by the black plot in Fig. 8. Drop in height (valleys) correspond to the dark lines, while peaks to the light regions in between. This means that the dark lines as seen by eye/optical microscope are actually furrows. This is also reflected in roughness values: about 14 µm across the furrows, and 2.2 – 4.7 µm along. The peak-to-valley distance in this case is about 70 µm, as seen in Fig.8, significantly larger than in sample 4.

Table 3. Summary of average inner surface roughness values and average peak-to-valley distances for all four samples.

Sample	Roughness (µm)	Peak-to-valley (µm)
1	2 – 14	17 – 70
2	1.5 – 2	10 – 15
3	1.1 – 2	9 – 26
4	2.5 – 5.5	15 – 28

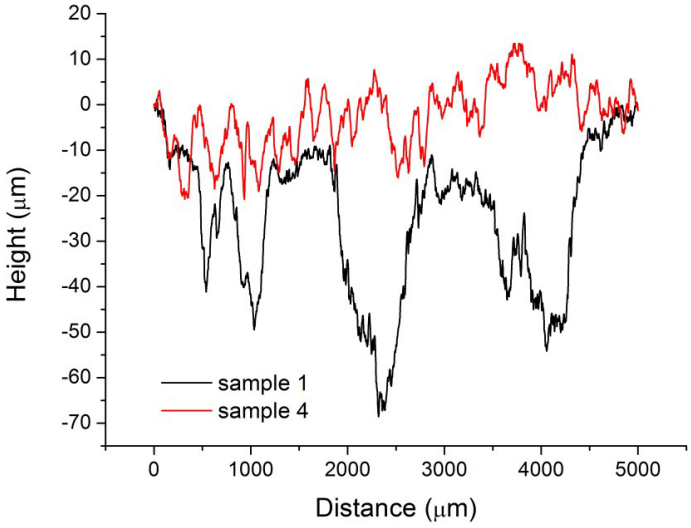

Fig. 8. Surface height profiles of samples 1, across the lines as seen in Fig.2(a,b), and sample 4.

5. Discussion

The present work consists of a detailed characterization of stainless steel pipeline material from the Ketzin pilot site. Both straight and bent pipe sections with different proximity to heating equipment had been collected from the site during decommissioning (see Fig. 1). During CO_2 injection the samples had been subjected to different conditions with regard to temperature and CO_2 phase conditions (see Tab. 1).

Little corrosion was visible on the pipe surfaces by optical inspection (Fig. 2), and the pipeline can thereby be said to have withstood the environment to which it had been exposed during the five years of CO_2 injection. Various SEM techniques and a profilometer were used to map the surface structure at micro-scale, chemistry and roughness of the pipe sections. This revealed some signs of corrosion over the whole inner surface for all samples, especially in

the bent sections of samples 1 and 2 (Figs. 2 and 4). It is expected that the bent region of the pipe is most severely attacked by corrosion, as the pipe bending procedure usually involves production of stresses in the material. These bending stresses are especially severe if the pipe is cold formed [14]. In a bent region the material will be subjected to tensile stresses which are known to enhance corrosion in stainless steels [15].

The deep furrows (up to 70 μm) at the bent section of sample 1 are unlikely to be caused by the flow pattern of the CO_2 mixture through so-called erosion corrosion [16], since the furrows exist evenly distributed on the inner surface of the bent section and not at all in the straight sections. These furrows may have originated from the initial pipe processing, and subsequently corroded due to CO_2 flow. In addition, it would not be expected to observe a high degree of erosion with a fluid composition with just a small amount of (or no) solid particles. A possible explanation for the increased corrosion on the sharp section of the bend in sample 1 is that the process is dependent on adsorption of molecules to the surface, a process which again could be dependent on the fluid velocity or phase (liquid vs gaseous).

The sample collected close to the inlet of the ambient air heater (Sample 1) was the most corroded one (Fig. 4). This sample was exposed to liquid CO_2 and subject to lowest temperatures (about -15°C) and most constant temperature conditions during operation. Sample 2 which was also exposed to liquid CO_2 but ambient temperature and its natural fluctuations, was the second most corroded sample. Samples 3 and 4, where gaseous CO_2 with higher temperatures (about 30 to 45°C) had flowed during standard operation, exhibited lower degree of corrosion. Physically, this could be based in a higher activity of residual water and formation of carbonic acid. Higher temperatures in contrast correlate with lower corrosion, which supports the former hypothesis.

Intergranular corrosion was the dominant form of corrosion, but some pitting corrosion was also observed (Fig. 5). The intergranular regions were either voids or including particles containing carbon and oxygen (Fig. 6). Auger spectroscopy indicated that the protective chromium oxide layer was severely damaged (Fig. 7). As seen in Figs. 5 and 7, some grains are more severely attacked by pitting corrosion than others. This is likely to be coupled to the grain orientation, as some crystal orientations are more susceptible to corrosion than others [17].

6. Conclusion

The present work has involved a detailed characterization of CO_2 pipeline materials collected after about five years of CO_2 exposure from the Ketzin pilot site in Germany. Various SEM techniques have been used to study the structure and chemistry of the inner and outer pipe surfaces, while a profilometer has been used to quantify pipe surface roughness. Little surface corrosion could be seen inside the pipe by optical inspection. At the micro-scale, however, it was found that the protective chromium oxide layer was cracked for all samples and severely eroded in some sections. The corrosion depth was typically no more than ~30 μm, which indicates an ongoing slow corrosion process.

The intensity of corrosion mainly correlates with two factors. Highest corrosion occurred at the coldest parts of the injection system, in presence of *liquid* CO_2. Sections exposed to higher temperatures, in contrast, show less corrosion. Moreover, the samples from the colder sections are bent pipes, therefore these may have an intrinsically higher susceptibility for corrosion due to the bending process prior to CO_2 flow. A weighting between these two potential processes cannot be given at this point. Although some furrows exist, their distribution indicates that erosion corrosion is not an important factor.

Yet, the main conclusion from this work is that the chosen pipeline material was sufficiently resistant to CO_2 corrosion for its purpose. As it is difficult to predict whether or not prolonged CO_2 exposure would cause non-linear corrosion rates our results suggest that care should be taken to protect bent pipeline sections and pipe sections exposed to low temperatures/liquid CO_2 when similar metals/conditions are used for longer operational lifetimes.

Acknowledgements

Financial support for this work was from the Norwegian Gassnova-funded project "Improving CO_2 well integrity by studies of materials from Ketzin wells", which is an add-on to the German COMPLETE project which is funded by the Federal Ministry of Education and Research, OMV, RWE, Vattenfall, VGS and Statoil. The authors would like to thank Tone Anzjøn for cutting the samples and John Walmsley for SEM support, both at SINTEF Materials and Chemistry. We also acknowledge NTNU NanoLab and NTNU Department of Electronics and Telecommunications for the use of their experimental equipment.

References

[1] International Energy Agency (IEA), Energy Technology Perspectives (2012).
[2] United States Department of Energy (US DOE), Interagency Task Force on Carbon Capture and Storage (2012), Washington DC, USA.
[3] Dugstad A, Morland B. Is the corrosion risk in the pipeline underestimated? –Lack of reliable data is a reason for concern!, presented at the 7th Trondheim CCS Conference (TCCS7), 4-6 June 2013. Abstract located at: http://programme.exordo.com/tccs-7/
[4] Aursand P, Hammer M, Munkejord ST, Wilhelmsen Ø. Pipeline transport of CO_2 mixtures: Models for transient simulation. Int J Greenhouse Gas Control 2013; 15: 174-185; doi: 10.1016/j.ijggc.2013.02.012.
[5] Dugstad A, Clausen S, Morland B. Transport of dense phase CO_2 in C-steel pipelines – when is corrosion an issue? NACE Corrosion conference and expo 2011, N0. 11070.
[6] He W, Knudsen OØ, Diplas S. Corrosion of stainless steel 316L in simulated formation water environment. Corrosion Science 2009; 51: 2811-2819.
[7] Klinkby L, Nielsen CM, Krogh E, Smith IE, Palm B, Bernstone C. Simulating rapidly fluctuating CO_2 flow into the Vedsted CO_2 pipeline, injection well and reservoir. Int J Greenhouse Gas Control 2011; 4: 4291-4298; doi:10.1016/j.egypro.2011.02.379.
[8] Jäger A, Span R. Equation of state for solid carbon dioxide based on the Gibbs free energy. Journal of Chemical and Engineering Data 2012; 57, 2: 590-595.
[9] Li H, Jakobsen JP, Wilhelmsen Ø, Yan J. PVTxy properties of CO_2 mixtures relevant for CO_2 capture, transport and storage: review of available experimental data and theoretical models. Applied Energy 2011; 88, 113567-3579.
[10] Martens S, Kempka T, Liebscher A, Lüth S, Möller F, Myrttinen A et al. Europe's longest-operating on-shore CO_2 storage site at Ketzin, Germany: A progress report after three years of injection. Environ Earth Sci 2012; 67: 323-334. doi: 10.1007/s12665-012-1672-5.
[11] Martens S, Liebscher A, Möller F, Henninges J, Kempka T et al. CO_2 storage at the Ketzin pilot site: Fourth year of injection, monitoring, modelling and verification. Energy Procedia 2013; 37: 6434-6443. doi:10.1016/j.egypro.2013.06.573.
[12] Liebscher A, Möller F, Bannach A, Köhler S, Wiebach J, Schmidt-Hattenberger C, Weiner M, Pretschner C, Ebert K., Zemke J. Injection operation and operational pressure-temperature monitoring at the CO_2 storage pilot site Ketzin, Germany - Design, results, recommendations. Int J Greenhouse Gas Control 2013; 15: 163-173. doi:10.1016/j.ijggc.2013.02.019.
[13] Martens S, Moeller F, Streibel M, Liebscher A, the Ketzin Group. Completion of five years of safe CO_2 injection and transition to the post-closure phase at the Ketzin pilot site. Energy Procedia 2014; in press.
[14] European Stainless Steel Development Association, Bending stainless steel tube - Design benefits in engineering and architecture. Materials and Application Series, Volume 15. ISBN 978-2-87997-045-5, http://www.aceroplatea.es/docs/comites/documento5_82.pdf.
[15] Gullberg D. Influence of composition, grain size and manufacture process on the anisotropy of tube materials. Master thesis printed by Ångstrømlaboratoriet, Uppsala Universitet. ISSN: 1401-5773.
[16] Muhammadu MM, Sheriff JM, Hamzah E. Effect of Flow Pattern at Pipe Bends on Corrosion Behavior of Low Carbon Steel and its Challenges, Jurnal Teknologi (Sciences & Engineering) 2013; 63, 1: 55-65.
[17] Lauvstad GØ, Johnsen R, Borck Ø, Falck da Silva E, Walmsley J. Breakdown in passivity of austenitic stainless steels in Cl^- and H_2S – Modelling and characterization of the pit initiation process. NACE International Corrosion Conference & Expo. 2007, Paper 07660.